Integrate InSAR and GPS for Crustal Deformation Mapping

Zhen Liu (JIFRESSE, UCLA)
Co-I: Zheng-Kang Shen (UCLA)

1. Summary

Towards developing a combined 3-D deformation field from a joint analysis of InSAR and GPS data, we have developed a new approach to integrate InSAR and GPS velocities for optimal 3-D deformation field and more rigorous ways to account for the interpolated GPS velocity uncertainties and uncertainties associated with InSAR deformation map. We have applied the new approach to four descending and ascending tracks in SCEC region and show that combining InSAR and GPS improves the resolution of deformation signals especially in the vertical direction. Our study shows the inclusion of InSAR not only improves the small scale deformation signals but also help better resolves broad uplift signals observed in the East California Shear Zone and Mojave desert, which probably relates to postseismic processes following past seismic events. The overall similar vertical pattern with and without use of GPS vertical constraint suggest these features are robust and likely results from a combination of tectonic and non-tectonic deformation sources. We presented the results from InSAR and GPS integration at 2017 SCEC Annual Meeting and 2018 SCEC CGM workshop held in March 2018 at Scripps Institute of Oceanography. One manuscript about integration method and application is in preparation.

2. Technical Report

Compared to GPS, InSAR line-of-sight measurements have dense spatial resolution, are more sensitive to vertical and 1-D. In comparison, point-based GPS measurements provide 3-D displacement components, are highly accurate in horizontal but less accurate in vertical, and are limited when resolving small-scale deformation processes depending on station distribution and spacing. It is expected that a combination of the two will improve both horizontal and in particular vertical as well as fine-scale surface motion features.

We have developed a method to integrate InSAR and GPS data for optimal 3-D deformation mapping. To combine InSAR and GPS data, we first divide the study area into regularly spaced grid cells. We then interpolate point-based discrete GPS measurements into continuous 3-D vector map at the regularly spaced grids with realistic estimation of data uncertainties. For GPS data, we do interpolation and uncertainty estimates in two separate steps. The interpolation is based on an algorithm developed by Shen et al. [2015] that takes into account GPS station distance, network density and configuration. At each grid point GPS data in its vicinity are interpolated to derive velocity, strain rate, and rotation rate through a least-square regression. The data are weighted based on their distance to the site and the voronoi cell areas occupied. The amount of weighting can be spatially variable and optimally determined based on in situ data strength. Less degree of smoothing is imposed for sites with denser local GPS network thus better spatial resolution can be achieved, and vice versa. For the uncertainties of the interpolated velocities, a Gaussian distance weighting parameter is taken to be a constant for all the grid points, to ensure that the a priori treatment of the weighting is uniformly applied to all the interpolation points, and the solution uncertainties deduced reflect not the relative a priori contribution but the relative data

strengths. For InSAR, we adopt a Jackknife variance estimation approach [Efron and Stein, 1981] to characterize the uncertainties associated with InSAR deformation map. The Jackknife approach provides a reasonable way to account for uncertainties caused by lacking or missing dates, uncorrected residual or other noises, and/or the influence of reference pixel and date. But it may underestimate the uncertainties due to spatially correlated noise. We therefore impose a minimum uncertainty of 1 mm/yr to account for uncertainties that are not accounted for. We average the InSAR LOS velocities for all pixels in each grid cell and propagate the uncertainty of each pixel to yield the uncertainty for each grid cell. When multiple images of InSAR LOS data are used, we estimate their relative offsets and ramp errors through an overall least-squares regression. There is also an option whether to estimate offset only or offset and ramp in the procedure.

Finally, we combine GPS and InSAR at each grid cell and solve for optimal 3-D components. All the InSAR data at each cell (single or multiple) are used together with the GPS to solve for the 3D displacements in a least-squares inversion. The InSAR data are weighted by their uncertainties, with the option of using the realistic uncertainty estimate or a default value. The GPS data are also weighted by their realistic uncertainties. In the combination we make the use of GPS vertical as optional for constraining the solution.

In our current effort, we applied the approach to a composite GPS velocity field that we compiled using continuous GPS (CGPS) velocities and campaign GPS velocities from SCEC CMM4 [Shen et al., 2011] (Figure 1), and InSAR line-of-sight (LOS) velocities from four descending and ascending tracks covering large portion of the SCEC region

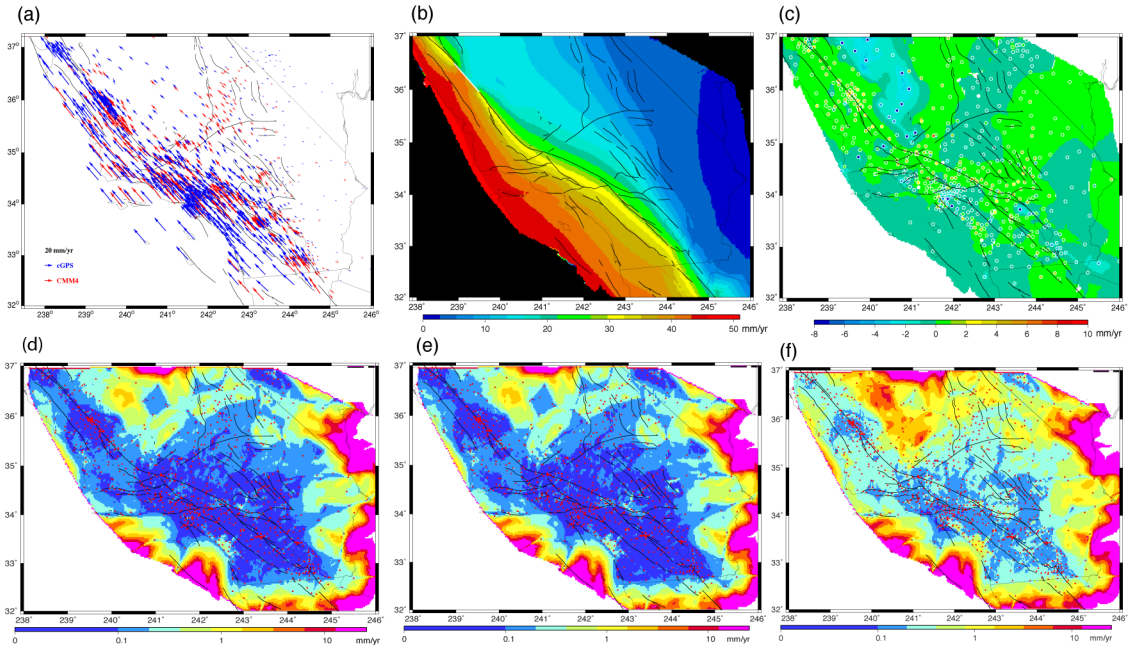

Figure 1. (a) Composite GPS velocities in SNARF reference frame that are used in the combination with InSAR data. (b) Contour plot of interpolated horizontal velocity field; (c) GPS vertical observations (filled circles) and interpolated vertical velocity field. (d) (e) and (f) Uncertainties of east, north, up components of interpolated GPS velocities. The CGPS velocities are rotated to align with the CMM4 solution and referenced to the SNARF reference frame. Both data sets are screened to remove outliers.

(Figure 2). Figure 1 shows interpolated GPS velocity uncertainties are, as expected, smaller at places with denser GPS data while uncertainties are larger at locations with less dense GPS data (e.g., outer boundary of GPS network).

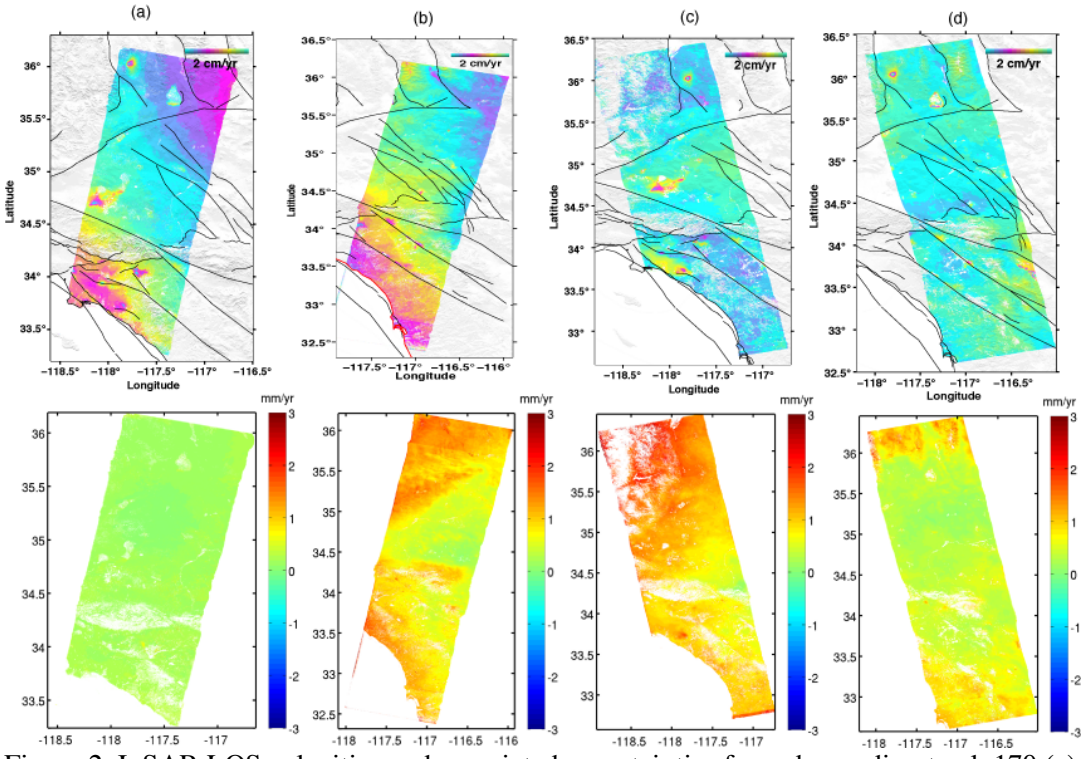

Figure 2. InSAR LOS velocities and associated uncertainties from descending track 170 (a), 399(b), and ascending track 120(c) and 349(d) that are used in the combination. Top row: LOS velocities. Bottom row: respective uncertainties.

Our results show that the scattering and uncertainties in GPS vertical and coarse nature of GPS measurements prevents resolving small-scale deformation signals. Inclusion of InSAR measurement clearly improve the resolution of such signals in the vertical direction (Figure 3, 4 and 5). We find that the combined horizontal velocity field does not change much between the combination that use GPS vertical as constraint (Figure 4) and the combination without the use of GPS vertical (Figure 3), probably because the horizontal deformation field is quite smooth and horizontal components of local deformation sources is small. The post-fit residuals from 3-D combination is about 1.1 mm/yr, slightly larger than the minimum uncertainty we impose during the inversion. Note that the inclusion of InSAR not only improves the small scale deformation signals but also help better resolves broad uplift signals observed in the East California Shear Zone and Mojave desert, which may be due to postseismic deformation processes following past seismic events. These areas are characterized by coarse GPS station distribution.

The overall similar vertical pattern in Figure 3 and 4 suggest these features are robust and likely results from a combination of broad tectonic and local non-tectonic deformation sources. We find that consideration of both InSAR offset and ramp in the combination improves the overall misfit residuals. However, ramp errors are typically small and concentrates in ascending tracks, which may be related to some unaccounted noise

sources such as ionosphere noises. Recent studies using sentinel-1 data suggest that C-band InSAR data in California is also subject to ionosphere noise, especially ascending track, and should be properly corrected (person. comm. with Cunren Liang).

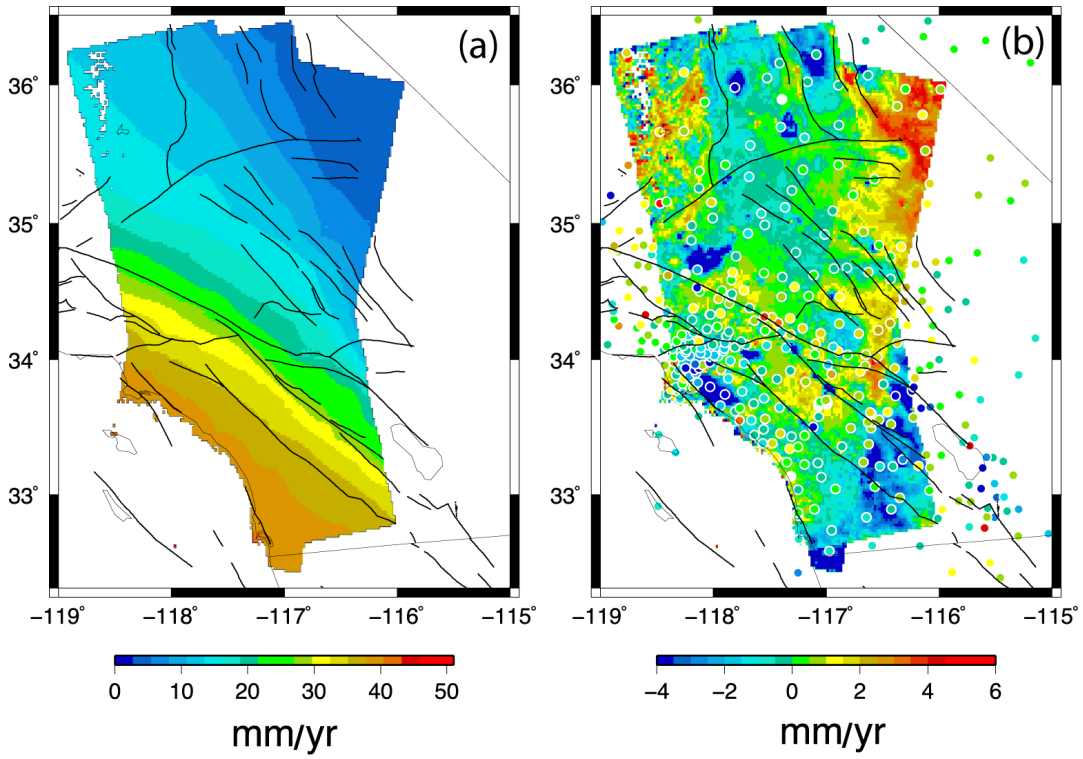

Figure 3. Combined 3-D velocities over the region covered by the InSAR tracks without use of GPS verticals in the combination. The relative offsets and ramp between InSAR tracks are estimated along with combined 3-D velocity field. Both InSAR and GPS interpolated velocity uncertainties are used. (Left) combined horizontal velocities. (Right) combined vertical velocities. The filled color circles are GPS verticals that are not used in the combination but overlaid for comparison. As compared with Figure 4, including InSAR without GPS vertical clearly improves resolving small-scale vertical deformation signals.

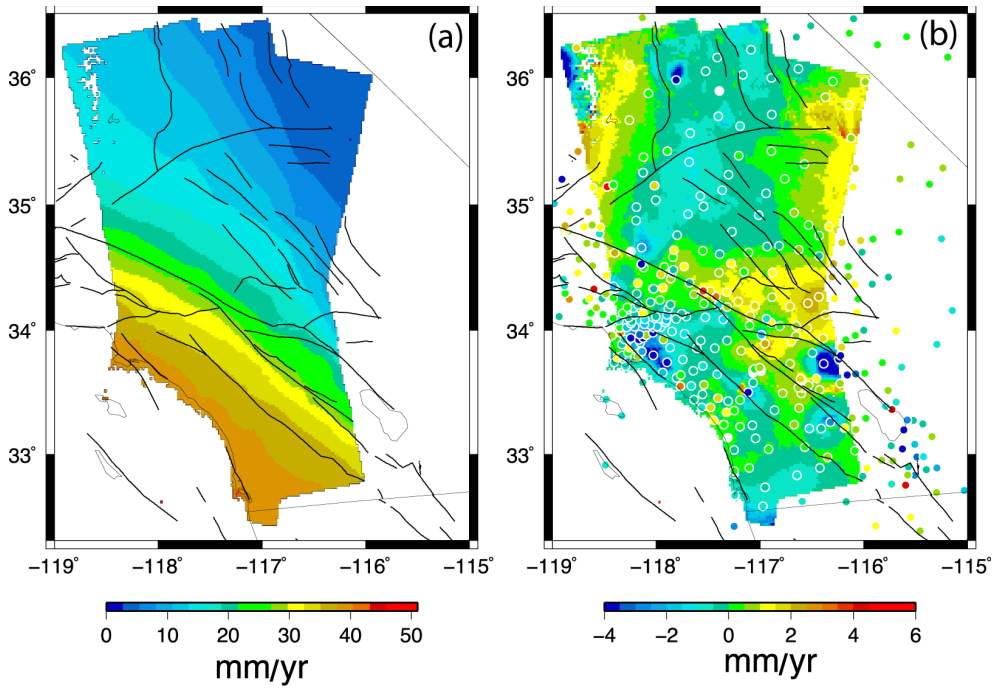

Figure 4. Combined 3-D velocities over the region covered by the InSAR tracks, but use GPS verticals in the combination. (Left) combined horizontal velocities. (Right) combined vertical velocities. Other captions are the same as Figure 3.

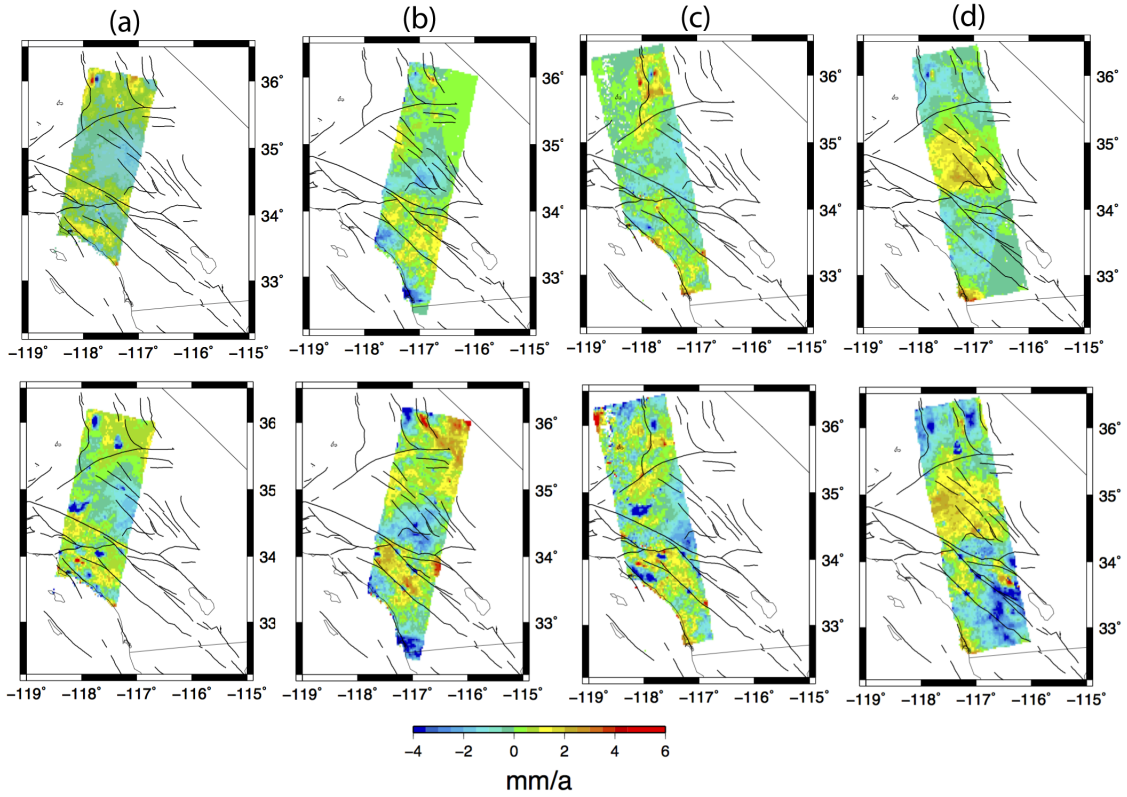

Figure 5. Residual InSAR LOS velocities after 3-D combination with GPS. (Top row) InSAR residuals of four tracks from 3-D combination that does not use GPS vertical constrain. (Bottom row) InSAR residuals of four tracks from 3-D combination that uses GPS vertical constraint. (a)-(d) represent track 170, 399, 120, 349, respectively.

6. Presentations and Publications

- Liu, Z., Shen, Z., Liang, C., & Lundgren, P. (2017, 08). Integration of InSAR and GPS data for 3-dimensional crustal deformation mapping. Poster Presentation at 2017 SCEC Annual Meeting. SCEC Contribution #7766
- Shen, Z., Liu, Z., Integration of InSAR and GPS data for crustal deformation mapping, manuscript in preparation.
- Gualandi, A., & Liu, Z. (2018, 08). Afterslip and Viscoelastic Processes and Their Relation with Seismic Activity: An Example from the Study of the Mw 7.2 El Mayor-Cucapah Earthquake (Mexico). Poster Presentation at 2018 SCEC Annual Meeting. SCEC Contribution #8565
- Chen, K., Smith, J., Avouac, J., Liu, Z., & Y. Tony, S. (2018, 08). Magma movement from Nāpau down to Leilani Triggered the 4th May 2018 Mw 7.0 Hawaii earthquake. Poster Presentation at 2018 SCEC Annual Meeting. SCEC Contribution #8664